Asia-Pacific Journal of Ophthalmology xxx (xxxx) xxx

Contents lists available at ScienceDirect

Asia-Pacific Journal of Ophthalmology

journal homepage: www.sciencedirect.com/journal/asia-pacific-journal-of-ophthalmology

Longitudinal evaluation of Bruch's membrane opening-minimum rim width in Chinese children: The Hong Kong Children Eye Study

Yi Li [a,1], Xiu Juan Zhang [a,b,1], Yuzhou Zhang [a], Ka Wai Kam [a,d], Alvin L. Young [a,d], Patrick Ip [e], Wei Zhang [f], Li Jia Chen [a,c,d,h], Clement C. Tham [a,c,d,g,h], Jost B. Jonas [i,j,k], Kyoko Ohno-Matsui [l], Chi Pui Pang [a,h], Jason C. Yam [a,c,d,g,h,*]

[a] Department of Ophthalmology and Visual Sciences, The Chinese University of Hong Kong, Hong Kong Special Administrative Region
[b] Department of Ophthalmology, LKS Faculty of Medicine, The University of Hong Kong, Hong Kong Special Administrative Region
[c] Hong Kong Eye Hospital, Kowloon, Hong Kong Special Administrative Region
[d] Department of Ophthalmology and Visual Sciences, Prince of Wales Hospital, Hong Kong Special Administrative Region
[e] Department of Paediatrics and Adolescent Medicine, Li Ka Shing Faculty of Medicine, The University of Hong Kong, Hong Kong Special Administrative Region
[f] Tianjin Eye Hospital, Tianjin Key Lab of Ophthalmology and Visual Science, Tianjin Eye Institute, Tianjin, China
[g] Department of Ophthalmology, Hong Kong Children Hospital, Hong Kong Special Administrative Region
[h] Hong Kong Hub of Paediatric Excellence, The Chinese University of Hong Kong, Hong Kong Special Administrative Region
[i] Institut Français de Myopie, Höpital Fondation Adolphe de Rothschild, Paris, France
[j] Singapore Eye Research Institute, Singapore
[k] Privatpraxis Prof Jonas und Dr Panda-Jonas, Heidelberg, Germany
[l] Department of Ophthalmology and Visual Science, Institute of Science Tokyo, Tokyo, Japan

ARTICLE INFO

Keywords:
Bruch's membrane opening-minimum rim width
Optical coherence tomography
Optic nerve head
Children

ABSTRACT

Purpose: To evaluate longitudinal changes in Bruch's membrane opening-minimum rim width (BMO-MRW) and its associated factors in school children aged 6–8 years, over 3 years, based on the Hong Kong Children Eye Study.

Methods: In this longitudinal study, 740 children received comprehensive ophthalmologic examinations at baseline and at 3-year follow-up visits. Based on their refractive status, they were divided into groups of persistent non-myopia, newly-developed myopia, and persistent myopia. Global and sectoral BMO-MRW, retinal nerve fiber layer (RNFL) thickness, BMO area, and disc area were all measured using spectral-domain optical coherence tomography (SD-OCT).

Results: The mean age of the participants at baseline was 7.71 ± 1.01 years (range 6–8 years), and 352 (47.7 %) were males. The 3-year follow-up visit revealed a significant increase in all sectors of BMO-MRW, average global BMO-MRW changed from 339.3 ± 51.7 μm to 361.3 ± 57.8 μm. Children in the persistent myopia group and newly developed myopia group showed significantly faster rates of BMO-MRW growth in all sectors compared to children of the persistent non-myopia group (all $P < 0.001$). In multivariable linear regression analysis, global BMO-MRW enlargement increased with larger axial length elongation ($\beta = 0.20$, $P < 0.001$), larger BMO area enlargement ($\beta = 0.21$, $P < 0.001$), and RNFL thickness thickening ($\beta = 0.45$, $P < 0.001$). It decreased with larger baseline BMO-MRW ($\beta = -0.17$, $P < 0.001$) and larger disc area enlargement ($\beta = -0.29$, $P < 0.001$).

Conclusions: Global and sectoral BMO-MRW increased over 3 years among school children aged 6–8 years, affected by larger axial elongation, larger BMO area enlargement, more marked RNFL thickening, and decrease in optic disc area.

* Correspondence to: Department of Ophthalmology and Visual Sciences, The Chinese University of Hong Kong, Hong Kong Eye Hospital, 147K Argyle Street, Kowloon, Hong Kong Special Administrative Region.
E-mail address: yamcheuksing@cuhk.edu.hk (J.C. Yam).
[1] Yi Li and Xiu Juan Zhang contributed equally as first authors.

https://doi.org/10.1016/j.apjo.2025.100219
Received 3 April 2025; Received in revised form 7 June 2025; Accepted 9 June 2025
Available online 19 June 2025

Introduction

Optic nerve head (ONH) assessment is useful in diagnosis of various ocular conditions in children, including pediatric glaucoma, optic nerve hypoplasia, and optic nerve atrophy.[1,2] With the rising global prevalence of axial myopia, there is increasing concern on corresponding escalation in glaucoma prevalence.[3] Moreover, diagnosing and evaluating glaucoma in individuals with high myopia can be difficult when using traditional methods like fundus photography and optical coherence tomography (OCT), especially on retinal nerve fibre layer (RNFL) thickness measurements. It is because myopic eyes often exhibit morphological changes in the peripapillary region, including parapapillary zones alpha, beta and gamma, shift of Bruch's membrane opening (BMO), and thinning of the peripapillary RNFL, all of which arise from marked myopic axial elongation.[4,5] Therefore, knowledge of physiological structural changes in the ONH during axial elongation in childhood is needed to facilitate an early identification of pathologic alterations, such as those occurring during the development of glaucomatous optic neuropathy.

Spectral domain-optical coherence tomography (SD-OCT) has emerged as a valuable tool for glaucoma diagnosis and monitoring in clinical practice. Comparing to ophthalmoscopic examination, it can better visualize and quantitatively evaluate ONH structures.[6] Besides the opening in the choroid and in the peripapillary scleral flange (covered by the lamina cribrosa), BMO is a part of the optic nerve head canal and causes physiologic defect in Bruch's membrane.[7] The BMO can be differentiated from the optic disc which may be defined as the ophthalmoscopically detectable part of the lamina cribrosa, covered by or free of neuroretinal rim. The minimum distance between the BMO margin and the internal limiting membrane (ILM), referred to as the Bruch membrane opening-minimum rim width (BMO-MRW), provides a more precise anatomical and geometric delineation of the neuroretinal rim compared to traditional techniques.[8] Previous observational studies[9,10] have highlighted the significance of the BMO-MRW in distinguishing glaucoma patients from normal control individuals, thereby enhancing the detection and diagnosis of glaucoma.

In contrast to known information on BMO-based parameters in adults,[10–13] few data are available regarding the BMO-MRW in children.[14,15] However, monitoring BMO-MRW in children is needed to know the changes in the ONH structure before and during myopia development. This information could shed light on the mechanisms and factors related to the myopia-associated changes of the ONH, as well as on the potential connection between myopia and glaucoma. Furthermore, observing BMO-MRW changes over time aids in the diagnosis of glaucoma, especially for children and adolescents at risk, such as high myopia. Cross-sectional studies have shown positive associations between older age and both BMO-MRW and RNFL thickness in children.[15–17] However, longitudinal investigations on the relationship between age and other factors with BMO-MRW and RNFL thickness in children and adolescents are still to be reported.

Accordingly, this study aimed to evaluate the characteristics of BMO-MRW in a cohort of Chinese children categorized by refractive status. Notably, the longitudinal changes of BMO-MRW, along with their associated factors in children prior to and during the early stage of myopia development, remain largely unknown. The data and information obtained may fill a gap in current knowledge of ONH structure changes during childhood, in particular with the concomitant development of myopia.

Methods

Study design and population

This prospective longitudinal study included participants of the Hong Kong Children Eye Study, a population-based study designed to document the occurrence and development of eye disorders in school children aged 6–8 years. Its details have been described in detail previously.[18–20] A group of children was randomly selected to participate in the current study applying SD-OCT.[15] The baseline examinations were conducted between January 2016 and July 2017, and follow-up examinations were performed 3 years afterwards. The study adhered to the Declaration of Helsinki, and ethical approval was obtained from the Institutional Review Board of the Chinese University of Hong Kong (CRE no. CRE2015.033). All children and their parents signed an informed consent form upon participation in the study.

Evaluation of BMO-MRW and ONH parameters using OCT

OCT optic nerve head (ONH) imaging was performed at baseline and 3-year follow-up, using Spectralis OCT (Heidelberg Engineering, Heidelberg, Germany). The ONH radial scan comprised 24 equally spaced radial B-scans, each comprising 768 A-scans, covering a 15° region centered on the optic disc. The fovea-to-BMO (FoBMO) axis was defined as the line connecting the fovea and the BMO centroid, while the FoBMO angle (θ) was defined as the angle between the FoBMO axis and the horizontal axis of the acquired image frame (AIF). BMO was defined as the innermost termination of Bruch's membrane and was assessed at 48 meridians across all B-scans of each eye. With the BMO points in each B-scan identified, the BMO-MRW values were defined as the shortest distance from each BMO point to the internal limiting membrane, yielding 48 values per eye. Only results from the standard ONH scans and the 3.5 mm diameter RNFL scans were analyzed. Both BMO-MRW and RNFL thickness were automatically calculated in global and sectors according to the Garway-Heath sectorization, including temporal (T), superior temporal (TS), superior nasal (NS), nasal (N), inferior nasal (NI), and inferior temporal (TI) segments (**Fig. 1**).

ONH parameters such as BMO area and disc area were calculated by the built-in algorithm automatically. The relationship between the measured size s on the OCT image (BMO area size and optic disc size) and its actual size t can be expressed by the formula $t = p \times q \times s$, where p represents the magnification factor related to the OCT camera and q is the magnification factor related to the eye. Given the default AL and refraction (zero D) for a magnification of 1 using the SD-OCT system, p can be calculated as 3.382. According to Bennett's formula, the q factor based on AL would be $0.01306 \times$ (AL - 1.82), where 1.82 is a constant. The magnification of the images was corrected by the Littmann-Bennett method; Littmann's "q-factor" was calculated by subtracting the value of 1.82 from the individual AL measurement, $t = 3.382 \times 0.01306 \times$ (AL - 1.82) $\times$ s.[21,22]

Quality control

OCT images with significant artifacts and poor image quality were excluded from analysis. All B-scans in this study had a quality score greater than 15. We included in the analysis the results obtained from one eye of each participant. We used images of the right eye unless they were excluded due to poor image quality or insufficient data. In this case, images of the left eye were used. The examiners were masked during the examination with respect to demographic and ocular parameters. Each B-scan of the OCT images was reviewed and verified by one trained reader (Y.L). Manual correction was performed if the automatic segmentation of BMO was incorrect or failed. In cases of doubt, a senior researcher (X.J.Z.) or an experienced ophthalmologist (J. C.Y.) was consulted.

Ocular and physical examinations

All participants underwent detailed ophthalmic and physical examinations at baseline and 3-year follow-up visits. Ocular biometry, including the measurement of axial length (AL) and corneal thickness, was performed using noncontact partial coherence laser interferometry (IOL Master; Carl Zeiss Meditec, Oberkochen, Germany). Cycloplegia

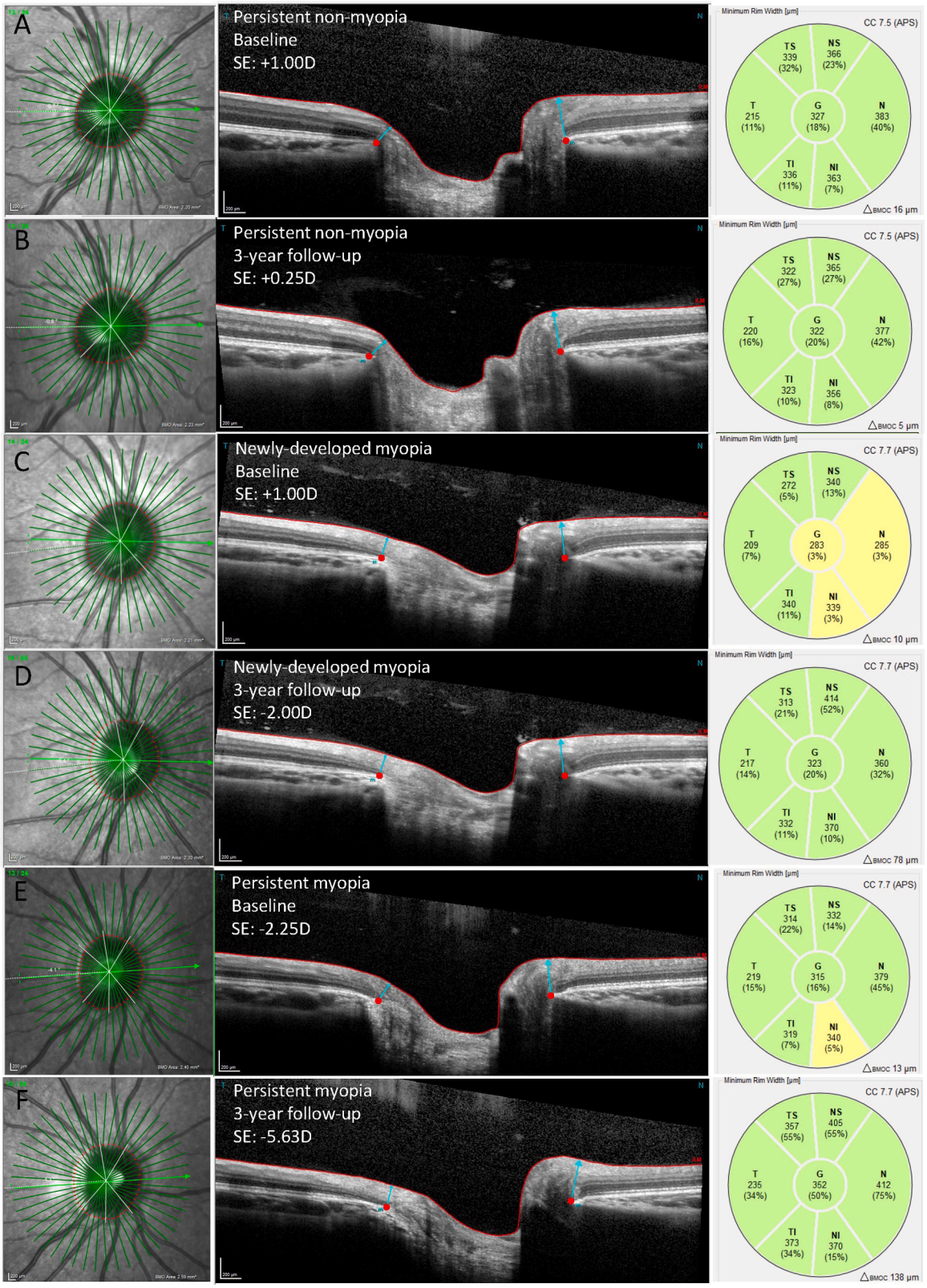

Fig. 1. OCT imaging of BMO-MRW in randomly selected participants with different refractive status. Horizontal b-scans obtained through optical coherence tomography (OCT) in the middle display the temporal and nasal Bruch's membrane opening-minimum rim width (BMO-MRW), indicated by the blue arrow. The location of the BMO is marked by the red dot. The global and regional BMO-MRW values, based on the six Garway-heath sectors, are automatically calculated. (A–B) OCT images for an 8-year-old child with spherical equivalence (SE) progressed from + 1.00 to + 0.25 D over 3 years (persistent non-myopia). (C-D) OCT images for a 6-year-old child with SE progressed from + 1.00 to − 2.00 D over 3 years (newly developed myopia). (E–F) OCT images for a 7-year-old child with SE progressed from − 2.25 to −5.63 D over 3 years (persistent myopia).

was achieved using a combination of eye drops containing 1 % cyclopentolate (Cyclogyl®; Alcon-Convreur Co, Rijksweg, Belgium) and eye drops containing 1 % tropicamide (Tropicamide®, Santen Co., Osaka, Japan), administered 5 min apart for each eye. This process was repeated for at least two cycles, with a 10-minute interval between each cycle. Based on the cycloplegic auto-refractometry, we calculated the spherical equivalent of the refractive error (SER) as the sum of the spherical power plus half of the cylindrical power of the refractive error. The changes in AL and SER were determined as the difference in the values obtained at the follow-up measurements minus the values measured at the study baseline. For physical examinations, the blood pressure of the children was measured using a digital automatic blood pressure monitor (Spacelabs Medical Co., Washington DC, USA), and the body height and weight were recorded using a professional integrated device (Seca Co., Hamburg, Germany).

Statistical analysis

Statistical analyses were conducted using the statistical software SPSS Statistics (version 27.0, IBM Co., Armonk, N.Y., USA). To compare continuous variables across different groups, a one-way analysis of variance was conducted, with Bonferroni correction applied for post hoc analysis. Differences in categorical variables were examined using chi-squared tests. This analysis included baseline and 3-year follow-up data. Participants were categorized into three refractive status groups: persistent non-myopia group (SER > -0.5 diopter at baseline and follow-up), newly-developed myopia (SER > -0.5 D at baseline and SER ≤ -0.5 D during the follow-up), and persistent myopia group (SER ≤ -0.5 D at baseline and follow-up). Pearson correlation analysis was used to evaluate the correlations between BMO-MRW and RNFL thickness. Moreover, the independent effects, including demographic factors and ocular parameters on the BMO-MRW change over 3 years (dependent variable), were evaluated by multivariable linear regression analysis. *P* values less than 0.05 were considered statistically significant.

Results

Study participants

The study was started with the cohort of the Hong Kong Children Eye Study, which consisted of 1226 children with a mean age of 7.79 ± 1.03 years. Among them, 400 were excluded from the present study due to loss of follow-up, 55 children were excluded due to poor OCT image quality, and 31 children due to incomplete data. The final analysis included 740 children, accounting for 60.4 % of the original population. Baseline characteristics of the included children are listed in Table 1. The mean age of participants was 7.71 ± 1.01 years, and 353 (47.7 %) of them were males. The SER of the eyes was 0.32 ± 1.30 D at baseline and progressed to − 1.29 ± 2.06 D during the 3-year follow-up. Of the participants, 288 children belonged to the persistent non-myopia group, 301 to the newly-developed myopia group, and 151 to the persistent myopia group. Age, axial length (AL), SER, BMO area, and height at baseline varied significantly among different groups (all $P \leq 0.001$). Participants in the current study were slightly older and less myopic compared to the overall cohort of the Hong Kong Children Eye Study, with no significant differences in other demographic and ocular characteristics (Supplementary Table 1). In addition, the characteristics of the included and excluded populations were comparable, although statistical differences were found in the comparisons of SE and AL, these differences were clinically small (Supplementary Table 2).

Changes in global and sectoral BMO-MRW over 3 years

The mean global BMO-MRW was 361.3 ± 57.8 μm at the 3-year follow-up, with a mean increase of 22.0 ± 33.8 μm (Table 2). The 3-year follow-up visit revealed a significant increase in BMO-MRW across all sectors, with the greatest sectoral BMO-MRW measurement in the inferior nasal sector (435.1 ± 74.1 μm), followed by the superior nasal sector (409.8 ± 77.1 μm). The eyes in the persistent myopia group and newly-developed myopia group exhibited a marked increase in BMO-MRW in all sectors compared to those in the persistent non-myopia group (all $P < 0.001$). Participants with longer AL at baseline (AL ≥ 23 mm) had a significantly larger enlargement of the BMO-MRW in the temporal and inferior temporal sectors as compared with participants with shorter AL (Supplementary Table 3).

Correlation of BMO-MRW changes with p-RNFL thickness change

Similar to BMO-MRW changes, RNFL thickness showed an increasing trend over the course of three years (Supplementary Table 4). The Pearson correlation coefficients (r) for pairs of sectoral BMO-MRW changes and p-RNFL thickness growth were r = 0.61 (global), 0.15 (temporal), 0.34 (temporal superior), 0.26 (temporal inferior), 0.52 (nasal), 0.48 (nasal superior), and 0.44 (nasal inferior). Significant correlations between BMO-MRW changes and RNFL thickness changes were observed in all sectors (all $P < 0.001$; Supplementary Table 5), with the strongest correlation between BMO-MRW change and RNFL thickness change in the nasal sector and the weakest in the temporal sector.

Associations of BMO-MRW growth with demographic and ocular parameters

The increase in global BMO-MRW over 3 years was associated with longer baseline AL, and with the increases in AL, BMO area, RNFL thickness (r = 0.17, 0.42, 0.41, and 0.61, respectively, all $P < 0.001$),

Table 1
Baseline characteristics of the study participants grouped by three refractive status.

	Total (n = 740)	(1) Persistent non-myopia (n = 288)	(2) Newly-developed myopia (n = 301)	(3) Persistent Myopia (n = 151)	*P* value	Post hoc
Age, years	7.7 (1.0)	7.6 (1.0)	7.6 (1.0)	8.1 (0.9)	**< 0.001**	1 = 2 < 3
Male sex (No%)	353 (47.7 %)	137 (47.6 %)	136 (45.2 %)	80 (53.0 %)	0.29	
Axial length, mm	23.1 (0.9)	22.7 (0.7)	23.0 (0.7)	23.8 (0.8)	**< 0.001**	1 < 2 < 3
Spherical equivalent refraction, D	0.3 (1.3)	1.2 (1.0)	0.4 (0.5)	− 1.6 (1.0)	**< 0.001**	1 < 2 < 3
Intraocular pressure, mmHg	15.8 (2.5)	15.8 (2.5)	15.7 (2.4)	16.1 (2.5)	0.35	
Central corneal thickness, μm	551.5 (30.9)	553.6 (31.4)	551.0 (30.0)	548.7 (31.2)	0.28	
FoBMO angle	− 5.9 (3.9)	− 6.3 (3.8)	− 5.6 (4.0)	− 5.7 (4.0)	0.08	
BMO area, mm^2	2.2 (0.5)	2.2 (0.5)	2.2 (0.5)	2.3 (0.5)	**0.001**	1 < 3
Disc area, mm^2	2.2 (0.4)	2.1 (0.4)	2.2 (0.4)	2.2 (0.5)	**0.03**	1 < 2
Systolic blood pressure, mmHg	102.3 (10.7)	102.6 (10.4)	102.4 (11.0)	101.8 (10.7)	0.80	
Diastolic blood pressure, mmHg	65.7 (8.2)	66.1 (8.0)	65.7 (8.4)	65.1 (8.0)	0.48	

Results are presented as mean (SD) for quantitative variables and number (percentage) for categorical variables. Male sex was compared using a chi-squared test. Continuous variables were compared using ANOVA. Bonferroni correction was used for post hoc analysis.
Values in bold are statistically significant ($P < 0.05$).

Table 2
Longitudinal changes of global and sectoral Bruch's membrane opening-minimum rim width (BMO-MRW) in different refractive status groups.

	Total	(1) Persistent non-myopia	(2) Newly-developed myopia	(3) Persistent myopia	*P* value	Post hoc
Global BMO-MRW, μm						
Baseline	339.3 (51.7)	341.2 (53.9)	333.9 (46.2)	346.6 (56.8)	**0.04**	2 < 3
Follow-up	361.3 (57.8)	348.2 (54.3)	365.8 (56.3)	377.3 (62.1)	**< 0.001**	1 < 2 = 3
3-year change	22.0 (33.8)	7.0 (25.3)	31.9 (33.8)	30.7 (37.5)	**< 0.001**	1 < 2 = 3
Location						
Temporal, μm						
Baseline	245.7 (42.8)	249.6 (46.7)	240.9 (38.0)	247.9 (43.4)	**0.04**	1 > 2
Follow-up	258.0 (42.2)	251.5 (41.4)	258.0 (39.7)	270.3 (45.8)	**< 0.001**	1 = 2 < 3
3-year change	12.3 (25.5)	2.0 (20.1)	17.1 (25.4)	22.4 (28.1)	**< 0.001**	1 < 2 = 3
Superior Temporal, μm						
Baseline	329.0 (55.7)	333.6 (62.3)	324.3 (49.4)	329.7 (53.8)	0.13	
Follow-up	348.8 (59.2)	340.2 (59.0)	351.3 (56.2)	360.3 (63.4)	**0.002**	1 < 3
3-year change	19.8 (35.6)	6.6 (30.6)	27.1 (34.6)	30.6 (39.0)	**< 0.001**	1 < 2 = 3
Inferior Temporal, μm						
Baseline	378.5 (60.0)	382.7 (64.2)	372.2 (53.2)	383.1 (63.5)	0.06	
Follow-up	394.5 (65.1)	383.8 (64.6)	394.1 (61.0)	415.6 (69.1)	**< 0.001**	1 = 2 < 3
3-year change	16.0 (37.5)	1.2 (23.8)	21.9 (39.5)	32.5 (44.0)	**< 0.001**	1 < 2 < 3
Nasal, μm						
Baseline	361.9 (66.4)	360.4 (63.4)	355.4 (63.5)	377.5 (75.0)	**0.003**	1 = 2 < 3
Follow-up	393.8 (78.6)	373.6 (69.3)	404.4 (79.6)	411.1 (85.2)	**< 0.001**	1 < 2 = 3
3-year change	31.9 (53.1)	13.2 (41.8)	49.0 (51.8)	33.6 (62.5)	**< 0.001**	1 < 3 < 2
Superior Nasal, μm						
Baseline	383.0 (69.0)	385.5 (73.1)	378.9 (63.3)	386.6 (71.6)	0.39	
Follow-up	409.8 (77.1)	393.5 (73.4)	415.8 (75.9)	429.0 (80.6)	**< 0.001**	1 < 2 = 3
3-year change	26.8 (45.3)	8.02 (35.8)	36.9 (45.0)	42.3 (49.7)	**< 0.001**	1 < 2 = 3
Inferior Nasal, μm						
Baseline	416.0 (66.6)	418.7 (67.8)	410.6 (60.7)	421.8 (74.6)	0.17	
Follow-up	435.1 (74.1)	423.1 (71.4)	438.2 (72.1)	451.9 (79.2)	**< 0.001**	1 < 2 = 3
3-year change	19.1 (40.7)	4.4 (29.4)	27.6 (42.1)	30.1 (47.6)	**< 0.001**	1 < 2= 3

Comparison performed using 1-way analysis of variance test with post hoc test (Bonferroni) to compare differences among 3 groups. Values in bold are statistically significant ($P < 0.05$).

and the decreases in disc area and thin baseline global BMO-MRW (r = -0.29 and − 0.13, all $P < 0.001$, Supplementary Table 6).

The multivariable linear regression analysis (Table 3) showed that global BMO-MRW enlargement increased with AL elongation after 3 years (β = 0.20, $P < 0.001$; Fig. 2), BMO area enlargement (β = 0.21, $P < 0.001$), and RNFL thickening (β = 0.45, $P < 0.001$), and decreased with baseline BMO area (β = − 0.17, $P < 0.001$) and disc area enlargement (β = − 0.29, $P < 0.001$). The analysis also found that BMO area enlargement over 3 years increased with baseline BMO area (β = 0.14, $P < 0.001$), AL elongation (β = 0.58, $P < 0.001$), and disc area enlargement (β = 0.21, $P < 0.001$).

Discussion

In this population-based longitudinal study on Chinese children, the BMO-MRW, measured globally and sectorially, increased with larger

Table 3
Associations between demographics and ocular parameters with changes in global BMO-MRW or changes in BMO area.

	Non-standardized β	Standardized β	95 %CI		*P*	VIF
Model 1: Changes of Global BMO-MRW ($R^2 = 0.586$)						
Baseline Global BMO-MRW	− 0.17	0.27	− 0.21	− 0.13	**< 0.001**	1.618
Baseline BMO area	− 12.07	− 0.17	− 16.61	− 7.53	**< 0.001**	1.652
Baseline RNFL thickness	0.33	0.09	0.11	0.55	**0.003**	1.430
AL change	11.45	0.20	7.06	15.85	**< 0.001**	2.203
RNFL thickness change	2.87	0.45	2.52	3.22	**< 0.001**	1.211
BMO area change	39.71	0.21	24.77	54.66	**< 0.001**	2.440
Disc area change	− 50.46	− 0.29	− 60.36	− 40.57	**< 0.001**	1.256
Model 2: Changes of BMO area ($R^2 = 0.623$)						
Baseline AL	0.02	0.09	0.01	0.03	**< 0.001**	1.101
Baseline BMO area	0.05	0.14	0.03	0.07	**< 0.001**	1.353
Baseline Global BMO-MRW	0.00	0.10	0.00	0.00	**0.001**	1.312
AL change	0.18	0.58	0.16	0.20	**< 0.001**	1.409
RNFL thickness change	0.00	0.07	0.00	0.00	**0.023**	1.696
Disc area change	0.19	0.21	0.14	0.24	**< 0.001**	1.302
Global BMO-MRW change	0.00	0.19	0.00	0.00	**< 0.001**	2.299

Model 1 (Outcome: changes of global BMO-MRW; Method: Stepwise) adjusted for age, sex, follow-up time, systolic blood pressure, diastolic blood pressure, baseline AL, baseline global BMO-MRW, baseline RNFL thickness, baseline BMO area, FoBMO angle, intraocular pressure, AL change, BMO area change, disc area change, RNFL thickness change;

Model 2 (Outcome: changes of BMO area; Method: Stepwise) adjusted for age, sex, follow-up time, systolic blood pressure, diastolic blood pressure, baseline AL, baseline global BMO-MRW, baseline RNFL thickness, baseline BMO area, FoBMO angle, intraocular pressure, AL change, global BMO-MRW change, disc area change, RNFL thickness change.

Baseline optic disc area was not adjusted in the multivariable models due to high collinearity with baseline BMO area.

Values in bold are statistically significant ($P < 0.05$).

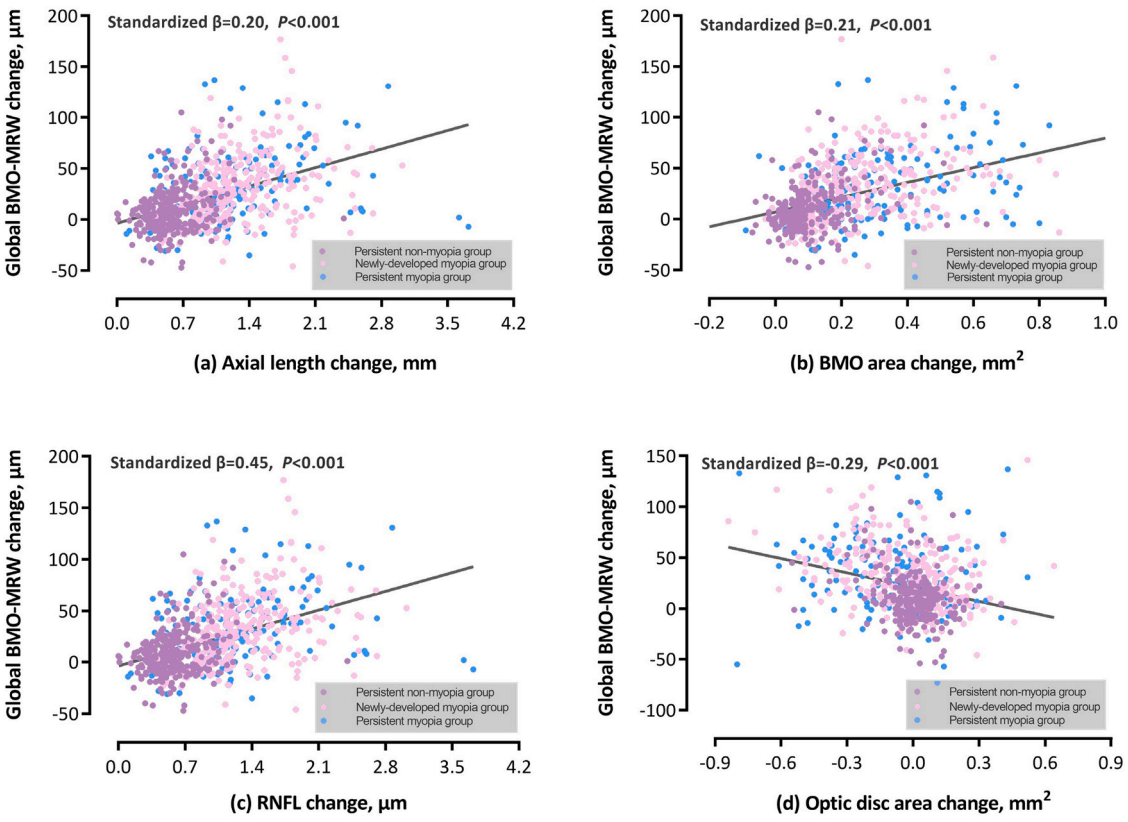

Fig. 2. Scatter plots showing associations between 3-year global BMO-MRW changes and ocular metrics. (a) Associations between global BMO-MRW changes and axial length elongation; (b) Associations between global BMO-MRW changes and BMO area enlargement; (c) Associations between global BMO-MRW changes and RNFL changes; (d) Associations between global BMO-MRW changes and disc area changes.

axial elongation, larger BMO area increase, more marked RNFL thickening, and decreased with larger baseline BMO-MRW and larger disc area enlargement during the study period. These findings may enhance our understanding of the longitudinal changes in BMO-MRW across different refractive status in children as well as facilitate more accurate ONH assessments for the early diagnosis of glaucoma and other optic neuropathy within clinical settings.

Some measurements made in this study concur with findings made in investigations by other research groups. The average global BMO-MRW measured in our study cohort increased from 339.5 µm to 361.3 µm at the 3-year follow-up. These values were higher than those previously reported for adults, with mean measurements ranging between 304 µm to 330 µm.[23–25] They were slightly lower than those reported previously for children in the USA with a mean axial length of 23.6 ± 0.9 mm, and for adolescents in Turkey, with a mean axial length of 23.4 ± 0.5 mm (mean BMO-MRW ranging between 371 µm and 374 µm).[14,26] In contrast to the age-related decrease in BMO-MRW observed in adults due to age-related loss of retinal ganglion cells and optic nerve fibers,[11] our study cohort noted an increasing trend of BMO-MRW in children. The enlargement of BMO-MRW may be attributed to several factors, including axon diameter increases, increase in glial tissue volume, and the maturation of the radial peripapillary capillary network during childhood.[16]

In the multivariable analyses, the BMO-MRW enlargement was associated with axial elongation. Previous histomorphometric and clinical studies on adults[24,27,28] showed that myopic axial elongation was associated with BMO enlargement, as the axial elongation-associated increase in the coronal diameters of the globe may increase the strain within Bruch's membrane in the posterior region. Hong et al.[16] noted a positive correlation between peripapillary RNFL thickness and axial length in children under 15 years old. Ha et al.[29] also reported an increase in temporal RNFL thickness in 36 children who experienced a myopia progression after a 4-year follow-up. On the other hand, neurodevelopmental data suggested that the human brain and neural circuits undergo dynamic changes throughout childhood and adolescence. Glial tissue volume may rise as a result of increased glial cell density, myelination of axons in the brain, and the growth and pruning of neural connections during this period.[30,31] Based on reported findings and results of the present study, we hypothesized that the positive correlation between BMO-MRW thickening and myopia progression could be attributed to the altered biomechanical properties of structures surrounding the ONH resulting from axial elongation.

Our results also suggested that disc area change was associated with BMO-MRW growth, which was partly consistent with a study on Korean adults[32] that reported significantly thinner BMO-MRW in the large discs (disc area $> 2.43\ mm^2$) than in the regular-sized discs (disc area: 1.63–2.43 mm^2). Previous studies[33] have revealed a curvilinear relationship between optic disc size and refractive status, with optic disc size being small in hyperopia and increasing towards emmetropia but decreasing from emmetropia to moderate myopia. In moderate myopia, axial elongation is associated with a shift of the BMO, typically towards the temporal direction. This shift contributes to the development of the gamma zone in the temporal parapapillary region and is associated with a shortening of the horizontal optic disc diameter. Consequently, there is a subsequent decrease in the optic disc area and a vertical ovalization of its shape.[33] The decreasing trend in optic disc size observed in our participants, as the majority of children in our study developed mild to moderate myopia during the follow-up visit, may also contribute to the increasing trend in BMO-MRW growth.

Also, in the present study, BMO-MRW and RNFL thickness were substantially linked at baseline and follow-up. Our results revealed variability sectorially across different groups of refractive status, with the strongest correlation between BMO-MRW change and RNFL thickness growth in the nasal (N) sector and the weakest in the temporal (T)

sector. This phenomenon could be attributed to the theory of incongruous growth patterns of sectoral BMO-MRW and RNFL thickness during axial elongation.[34] Axial elongation leads to a decrease in angle kappa, which is the angle between the temporal arterial vascular arcade. As a result, the RNFL in the temporal region gets thicker, while it becomes thinner in other regions, and the peaks of RNFL thickness distribution move in the direction of the temporal position.[35,36] These changes may explain the relatively weak correlation between RNFL and BMO-MRW in the temporal sector. Moreover, optic disc size may alter RNFL trajectories, leading to the observed variations in the relationship between sectoral BMO-MRW and RNFL thickness.[11,37] Other population-based studies[11,23,24] have reported modest correlations between global BMO-MRW and RNFL thickness in adults, however, the sectoral correlations were different compared to that of our results. In contrast, Jnawali et al. found no association between BMO-MRW and RNFL thickness in children aged 6–15 years.[26] Conflicting results between studies may be attributed to different age groups, sample sizes, refractive status, and ethnicities.

There are some limitations in our study. First, the age range of the included children was narrow (6–8 years), which limits exploration of potential associations of age with BMO-MRW in children. Second, the children in the persistent myopia group were older than those in the newly-developed myopia and persistent myopia groups, which may have influenced BMO-MRW measurements. However, our multivariable regression analysis revealed no correlation between age and BMO-MRW growth. Third, this study only included Chinese children, the applicability of our findings to other ethnic groups may be limited. Finally, our results should be interpreted with caution, as we did not account for the impact of ocular magnification on RNFL measurements. Although the diameter of the RNFL thickness scan circle is assumed to be consistent at 3.5 mm, the actual position of this measurement circle can vary due to ocular magnification, which is significantly influenced by axial length. The measured RNFL thickness would be underestimated in longer eyes, appearing thinner than its actual value. To evaluate the RNFL more accurately, adjusting for the effect of ocular magnification is recommended in future studies.

Conclusions

Both global and sectoral BMO-MRW significantly increased over a 3-year follow-up period in Chinese school children aged 6–8 years. The enlargement of BMO-MRW in the developing eye was associated with axial elongations and changes of BMO area, disc area and RNFL thickness. Our findings suggest that accounting for variations in axial length and ONH metrics is important when evaluating BMO-MRW values in children, adding to the potential application of BMO-MRW in the early detection of glaucoma and other optic neuropathies in pediatric populations.

Funding

This study was supported in part by the General Research Fund (GRF), Research Grants Council, Hong Kong (14102422 [JCY]); Collaborative Research Fund (C7149-20G [JCY]); Health and Medical Research Fund (HMRF), Hong Kong (11220206 [JCY], 10210246 [YZ], 09202466 [LJC]), National Natural Science Foundation of China (82425017 & 82171089 [JCY]); Strategic Impact Enhancement Fund, The Chinese University of Hong Kong (WW/SC/rc/SIEF2324/0366/24vw & TL/JF/rc/SIEF2223/0759/23vw [JCY]); the CUHK Jockey Club Children's Eye Care Programme (No grant number [JCY]); and the CUHK Jockey Club Myopia Prevention Programme (No grant number [JCY]).

Conflict of interest

No conflicting relationship exists for any author.

Acknowledgements

We would like to thank all the children and their families for their participation in the Hong Kong Children Eye Study.

Appendix A. Supporting information

Supplementary data associated with this article can be found in the online version at doi:10.1016/j.apjo.2025.100219.

References

1. Aizawa N, Kunikata H, Omodaka K, et al. Optic disc microcirculation in superior segmental optic hypoplasia assessed with laser speckle flowgraphy. *Clin Exp Ophthalmol*. 2014;42:702–704.
2. Gupta V, James MK, Singh A, et al. Differences in optic disc characteristics of primary congenital glaucoma, juvenile, and adult onset open angle glaucoma patients. *J Glaucoma*. 2016;25:239–243.
3. Marcus MW, de Vries MM, Montolio FG Junoy, et al. Myopia as a risk factor for open-angle glaucoma: a systematic review and meta-analysis. *Ophthalmology*. 2011;118:1989–1994. e1982.
4. Hsu CH, Chen RI, Lin SC. Myopia and glaucoma: sorting out the difference. *Curr Opin Ophthalmol*. 2015;26:90–95.
5. Jeong Y, Kim YK, Jeoung JW, et al. Comparison of optical coherence tomography structural parameters for diagnosis of glaucoma in high myopia. *JAMA Ophthalmol*. 2023;141:631–639.
6. Mwanza JC, Budenz DL. Optical coherence tomography platforms and parameters for glaucoma diagnosis and progression. *Curr Opin Ophthalmol*. 2016;27:102–110.
7. Chauhan BC, Burgoyne CF. From clinical examination of the optic disc to clinical assessment of the optic nerve head: a paradigm change. *Am J Ophthalmol*. 2013;156:218–227. e212.
8. Reis AS, Sharpe GP, Yang H, et al. Optic disc margin anatomy in patients with glaucoma and normal controls with spectral domain optical coherence tomography. *Ophthalmology*. 2012;119:738–747.
9. Chauhan BC, O'Leary N, AlMobarak FA, et al. Enhanced detection of open-angle glaucoma with an anatomically accurate optical coherence tomography–derived neuroretinal rim parameter. *Ophthalmology*. 2013;120:535–543.
10. Malik R, Belliveau AC, Sharpe GP, et al. Diagnostic accuracy of optical coherence tomography and scanning laser tomography for identifying glaucoma in myopic eyes. *Ophthalmology*. 2016;123:1181–1189.
11. Chauhan BC, Danthurebandara VM, Sharpe GP, et al. Bruch's membrane opening minimum rim width and retinal nerve fiber layer thickness in a normal white population: a multicenter study. *Ophthalmology*. 2015;122:1786–1794.
12. Gmeiner JM, Schrems WA, Mardin CY, et al. Comparison of Bruch's membrane opening minimum rim width and peripapillary retinal nerve fiber layer thickness in early glaucoma assessment. *Invest Ophthalmol Vis Sci*. 2016;57:OCT575–584.
13. Sanfilippo PG, Huynh E, Yazar S, et al. Spectral-domain optical coherence tomography-derived characteristics of bruch membrane opening in a young adult Australian population. *Am J Ophthalmol*. 2016;165:154–163.
14. Gedik AC, Ozbilen KT, Bayraktar S, et al. Bruch membrane opening-minimum rim width and retinal nerve fiber layer thickness in myopic children. *Photodiagn Photodyn Ther*. 2021;36, 102524.
15. Zhang XJ, Tang SM, Wang YM, et al. Increase in Bruch's membrane opening minimum rim width with age in healthy children: the Hong Kong children eye study. *Br J Ophthalmol*. 2022.
16. Hong SW, Ahn YJ, Kang NY. Relationship between age and retinal nerve fiber layer thickness in normal children. *Semin Ophthalmol*. 2017;32:655–660.
17. Zhang XJ, Lau YH, Wang YM, et al. Thicker retinal nerve fiber layer with age among schoolchildren: the Hong Kong children eye study. *Diagnostics*. 2022;12.
18. Yuan N, Li J, Tang S, et al. Association of secondhand smoking exposure with choroidal thinning in children aged 6–8 years: the Hong Kong children eye study. *JAMA Ophthalmol*. 2019;137:1406–1414.
19. Wong ES, Zhang XJ, Yuan N, et al. Association of optical coherence tomography angiography metrics with detection of impaired macular microvasculature and decreased vision in amblyopic eyes: the Hong Kong children eye study. *JAMA Ophthalmol*. 2020;138:858–865.
20. Yam JC, Tang SM, Kam KW, et al. High prevalence of myopia in children and their parents in Hong Kong Chinese population: the Hong Kong children eye study. *Acta Ophthalmol*. 2020;98:e639–e648.
21. Bennett AG, Rudnicka AR, Edgar DF. Improvements on Littmann's method of determining the size of retinal features by fundus photography. *Graefe's Arch Clin Exp Ophthalmol*. 1994;232:361–367.
22. Zhang XJ, Chau DKS, Wang YM, et al. Prevalence and characteristics of peripapillary gamma zone in children with different refractive status: the Hong Kong children eye study. *Invest Ophthalmol Vis Sci*. 2023;64(4).
23. Tun TA, Sun CH, Baskaran M, et al. Determinants of optical coherence tomography-derived minimum neuroretinal rim width in a normal Chinese population. *Invest Ophthalmol Vis Sci*. 2015;56:3337–3344.
24. Araie M, Iwase A, Sugiyama K, et al. Determinants and characteristics of Bruch's membrane opening and Bruch's membrane opening-minimum rim width in a normal Japanese population. *Invest Ophthalmol Vis Sci*. 2017;58:4106–4113.

25. Zheng F, Wu Z, Leung CKS. Detection of Bruch's membrane opening in healthy individuals and glaucoma patients with and without high myopia. *Ophthalmology*. 2018;125:1537–1546.
26. Jnawali A, Mirhajianmoghadam H, Musial G, et al. The optic nerve head, lamina cribrosa, and nerve fiber layer in non-myopic and myopic children. *Exp Eye Res*. 2020;195, 108041.
27. Zhang Q, Xu L, Wei WB, et al. Size and shape of Bruch's membrane opening in relationship to axial length, gamma zone, and macular Bruch's membrane defects. *Invest Ophthalmol Vis Sci*. 2019;60:2591–2598.
28. Jonas JB, Spaide RF, Ostrin LA, et al. IMI-nonpathological human ocular tissue changes with axial myopia. *Invest Ophthalmol Vis Sci*. 2023;64:5.
29. Ha A, Kim YK, Baek SU, et al. Longitudinal changes of circumpapillary retinal nerve fiber layer thickness profile during childhood myopia progression. *Sci Rep*. 2022;12:2555.
30. Tau GZ, Peterson BS. Normal development of brain circuits. *Neuropsychopharmacology*. 2010;35:147–168.
31. Milbocker KA, Campbell TS, Collins N, et al. Glia-driven brain circuit refinement is altered by early-life adversity: behavioral outcomes. *Front Behav Neurosci*. 2021;15, 786234.
32. Cho HK, Park JM, Kee C. Effect of optic disc size on correlation between Bruch's membrane opening-minimum rim width and peripapillary retinal nerve fibre layer thickness. *Eye*. 2019;33:1930–1938.
33. Jonas JB, Zhang Q, Xu L, et al. Change in the ophthalmoscopical optic disc size and shape in a 10-year follow-up: the Beijing eye study 2001–2011. *Br J Ophthalmol*. 2023;107:283–288.
34. Patel A, Purohit R, Lee H, et al. Optic nerve head development in healthy infants and children using handheld spectral-domain optical coherence tomography. *Ophthalmology*. 2016;123:2147–2157.
35. Jonas JB, Jonas RA, Bikbov MM, et al. Myopia: histology, clinical features, and potential implications for the etiology of axial elongation. *Prog Retin Eye Res*. 2022, 101156.
36. Zhang Q, Xu L, Zhao L, et al. Peaks of circumpapillary retinal nerve fibre layer and associations in healthy eyes: the Beijing eye study 2011. *Br J Ophthalmol*. 2022;106:1417–1422.
37. Jansonius NM, Schiefer J, Nevalainen J, et al. A mathematical model for describing the retinal nerve fiber bundle trajectories in the human eye: average course, variability, and influence of refraction, optic disc size and optic disc position. *Exp Eye Res*. 2012;105:70–78.